High Spectral Efficiency Long-Wave Infrared Free-Space Optical Transmission With Multilevel Signals

Mengyao Han, Mahdieh Joharifar [ID], Muguang Wang [ID], *Senior Member, IEEE*, Richard Schatz [ID], Rafael Puerta [ID], *Senior Member, IEEE*, Yan-ting Sun [ID], Yuchuan Fan [ID], Grégory Maisons, Johan Abautret, Roland Teissier, Lu Zhang [ID], Sandis Spolitis [ID], Vjaceslavs Bobrovs [ID], Sebastian Lourdudoss [ID], *Senior Member, IEEE*, Xianbin Yu [ID], *Senior Member, IEEE*, Sergei Popov [ID], Oskars Ozolins, *Senior Member, IEEE*, and Xiaodan Pang [ID], *Senior Member, IEEE*

Abstract—**This study explores the potential of long-wave infrared free-space optical (FSO) transmission that leverages multilevel signals to attain high spectral efficiency. The FSO transmission system consists of a directly modulated-quantum cascade laser (DM-QCL) operating at 9.15 μm and a mercury cadmium telluride (MCT) detector. To fully understand the system, we conduct measurements on the DM-QCL chip and MCT detector and assess the overall amplitude response of the DM-QCL, MCT detector, and all electrical components. We apply various signals, including on-off keying (OOK), 4-level pulse amplitude modulation (PAM4), 6-level PAM (PAM6), and 8-level PAM (PAM8) to maximize the bit rate and spectral efficiency of the FSO transmission. Through a two-dimensional sweeping of the laser bias current and MCT detector photovoltage, we optimize the transmission performance. At the optimal operation point, the FSO system achieved impressive results which are up to 6 Gbaud OOK, 3.5 Gbaud PAM4, 3 Gbaud PAM6, and 2.7 Gbaud PAM8 signal transmissions, with a bit error rate performance below 6.25% overhead hard decision-forward error correction limit when the DM-QCL operates at 10 °C. We also evaluate the eye diagrams and stability of the system to showcase its remarkable transmission performance. Our findings suggest that the DM-QCL and MCT detector-based FSO transceivers offer a highly competitive solution for the next generation of optical wireless communication systems.**

Index Terms—**Free-space optical communication, intensity modulation, long-wave infrared, quantum cascade laser.**

Mengyao Han is with the Institute of Lightwave Technology, Key Lab of All Optical Network and Advanced Telecommunication Network, Ministry of Education, Beijing Jiaotong University, Beijing 100044, China, and also with the Department of Applied Physics, KTH Royal Institute of Technology, 106 91 Stockholm, Sweden (e-mail: mengyaohan@bjtu.edu.cn).

Mahdieh Joharifar, Richard Schatz, Yan-ting Sun, Sebastian Lourdudoss, and Sergei Popov are with the Department of Applied Physics, KTH Royal Institute of Technology, 106 91 Stockholm, Sweden (e-mail: mahdieh@kth.se; rschatz@kth.se; yasun@kth.se; slo@kth.se; sergeip@kth.se).

Muguang Wang is with the Institute of Lightwave Technology, Key Lab of All Optical Network and Advanced Telecommunication Network, Ministry of Education, Beijing Jiaotong University, Beijing 100044, China (e-mail: mg-wang@bjtu.edu.cn).

Rafael Puerta is with the Department of Applied Physics, KTH Royal Institute of Technology, 106 91 Stockholm, Sweden, and also with the Ericsson Research, Ericsson AB, 164 83 Stockholm, Sweden (e-mail: rafael.puerta@ericsson.com).

Yuchuan Fan is with the Department of Applied Physics, KTH Royal Institute of Technology, 106 91 Stockholm, Sweden, and also with the RISE Research Institutes of Sweden, 164 40 Kista, Sweden (e-mail: yuchuanf@kth.se).

Grégory Maisons, Johan Abautret, and Roland Teissier are with the mirSense, 91120 Palaiseau, France (e-mail: gregory.maisons@mirsense.com; johan.abautret@mirsense.com; roland.teissier@mirsense.com).

Lu Zhang and Xianbin Yu are with the College of Information Science and Electronic Engineering, Zhejiang University, and Zhejiang Lab, Hangzhou 310027, China (e-mail: zhanglu1993@zju.edu.cn; xyu@zju.edu.cn).

Sandis Spolitis and Vjaceslavs Bobrovs are with the Institute of Telecommunications, Riga Technical University, 1048 Riga, Latvia (e-mail: sandis.spolitis@rtu.lv; vjaceslavs.bobrovs@rtu.lv).

Oskars Ozolins and Xiaodan Pang are with the Department of Applied Physics, KTH Royal Institute of Technology, 106 91 Stockholm, Sweden, and with the RISE Research Institutes of Sweden, 164 40 Kista, Sweden, and also with the Institute of Telecommunications, Riga Technical University, 1048 Riga, Latvia (e-mail: oskars.ozolins@ri.se; xiaodan@kth.se).

Color versions of one or more figures in this article are available at https://doi.org/10.1109/JLT.2023.3287934.

Digital Object Identifier 10.1109/JLT.2023.3287934

I. INTRODUCTION

THE rapid development of various emerging applications, such as eXtended Reality (XR), the Internet of Things, and artificial intelligence-aided smart applications, has posed a requirement on ultra-high speed data traffic in wireless communications [1]. The International Telecommunication Union (ITU) has projected that the volume of global mobile traffic will continue to rise significantly, reaching 5016 exabytes per month [2]. Indeed, supporting this extremely high-volume data produces a significant challenge for the fifth-generation (5G) and beyond wireless communication technologies. Radio frequency (RF)-based wireless communications are currently restricted by the shortage of spectrum resources and may not meet the ever-growing traffic requirement [3]. Free-space optical (FSO) communications, a distinct subset of optical wireless communications, can support high-speed data rate over long distances without exhausting the RF spectrum [4]. Furthermore, owing

to the laser beam with narrow and directional characteristics, the FSO system enables a high level of security, low power consumption, and immunity to electromagnetic interference [5]. Therefore, the study and development of the FSO system have attracted more and more study communities.

The two atmospheric transmission windows at the mid-wave IR (MWIR, 3–5 μm, 60–100 THz) and the long-wave IR (LWIR, 8–12 μm, 25–37 THz) are considered a potential resource for future FSO communications [6]. These two windows will be exploited as an alternative or complementary working spectrum to the current commercial FSO system [7], [8]. In addition, quantum optoelectronics devices, such as the quantum cascade laser (QCL) and quantum cascade detector (QCD), have been rapidly developed with broad modulation and detection bandwidth operating at room temperatures. The compact and high-speed solid-state FSO transmission system working at the MWIR and LWIR region has become possible [9]. Remarkably, a few kilometers of transmission distance of the laser beam at the LWIR region are achievable owing to the low molecular and aerosol scattering and high turbulence robustness at such long wavelengths [10].

Several LWIR FSO systems comprising QCL and QCD have recently been demonstrated with direct and external modulation schemes [11], [12], [13], [14], [15], [16], [17]. In [11], up to 10 Gbit/s FSO transmission was shown at 9 μm wavelength using a unipolar quantum optoelectronic system composed of a QCL, an external modulator, and a QCD. Very recently, thanks to the broader detection bandwidth of quantum-well-infrared photodetector (QWIP), the net data rates of 30 Gbit/s for on-off keying (OOK) and 4-level pulse-amplitude-modulation (PAM4) schemes are achieved with the bit error rate (BER) performance below the 27% overhead hard decision-forward error correction (OH HD-FEC) limit [12]. However, accurate beam alignment using extra LWIR lenses or mirrors is required to perform external modulation schemes. An LWIR FSO transmission with a bit rate of 11 Gbit/s was achieved based on a 9.6-μm directly-modulated quantum cascade laser (DM-QCL), and an uncooled and unbiased passive QCD has been reported in [13]. Both 8 Gbit/s OOK and 11 Gbit/s PAM4 signals are explored below the 6.25% OH HD-FEC limit. The DM-QCL provides a more efficient and straightforward candidate for accelerating commercial LWIR FSO solutions than the external modulation approach. In these works, however, the higher spectral efficiency transmission, e.g., 6-level PAM (PAM6) or 8-level PAM (PAM8) scheme, is limited by the stringent requirement for beam collimation and focusing due to the limited conversion efficiency of QCDs and QWIPs. Table I presents a comparative analysis of this work and several previously mentioned studies.

On the other hand, the mercury cadmium telluride (MCT) detectors usually have a wider operational spectral range covering from MWIR to LWIR region (2–12 μm), which can potentially enable wavelength division multiplexing without a dedicated detector design per wavelength. Although the detection bandwidth is limited, the MCT detectors are commercially available with fine-tuned collimation and low thermal noise performance, and often integrated with trans-impedance amplifiers (TIA). Such characteristics can improve the conversion efficiency and

TABLE I
COMPARISON OF MENTIONED EARLIER WORKS

Ref.	Architecture	Baudrate	FEC
[11]	QCL, external modulator, QCD	11 Gbaud OOK	7%-OH HD-FEC
[12]	QCL, external modulator, QWIP/QCD	24 Gbaud PAM4	27%-OH HD-FEC
[13]	DM-QCL, QCD	5.5 Gbaud PAM4	6.25%-OH HD-FEC
This work	DM-QCL, MCT detector	2.7 Gbaud PAM8	6.25%-OH HD-FEC

gain a higher signal-to-noise ratio (SNR) on the receiver side, indicating that the multilevel signals (PAM6, PAM8, etc.) can be applied to increase the FSO system's bit rate and spectral efficiency. Recently, with a DM-QCL and a commercial MCT detector, a 4 Gbit/s DMT signal has been demonstrated at the MWIR band, and the measured BER below 6.25% OH HD-FEC limit was achieved, enabled by the bit-loading scheme and frequency domain equalizer [14]. Besides, MWIR transmissions of up to 6 Gbit/s PAM8 signal with a BER performance below the 6.25% OH HD-FEC limit were also reported [15]. Furthermore, in [18] is reported the LWIR FSO transmission at 9.15 μm of 5G New-Radio (NR) signals fully compliant with the 3GPP RF conducted transmitter requirements, i.e., the adjacent channel leakage power ratio and the error vector magnitude, validating the high performance of MCT detector.

In this article, we extend our recent report on LWIR FSO transmission using a wideband MCT detector and a DM-QCL at 9.15 μm [19]. Compared with [19], we have made substantial extension by including the detailed characterization of the DM-QCL chip at varying operating temperatures, the use of various signals such as OOK, PAM4, and PAM6 to optimize the bit rate and spectral efficiency, the in-depth analysis of the BER performance with different decision-feedback equalizer (DFE) taps. A two-dimension sweeping is performed to identify the optimal operating point considering both the laser bias current and MCT detector photovoltage (PV). We experimentally compare four modulation formats, i.e., OOK, PAM4, PAM6, and PAM8, and benchmark their respective maximum data rate against the 6.25% OH HD-FEC limit [20]. By using pulse shaping, pre-, and post-digital processing technologies, up to 6 Gbaud OOK, 3.5 Gbaud PAM4, 3 Gbaud PAM6, and 2.7 Gbaud PAM8 signals are successfully transmitted at an operating temperature of 10 °C. All signals with BER performance below the 6.25% OH HD-FEC limit are achieved. Finally, the system stability is evaluated to show valuable references for practical applications.

The rest of this article is organized as follows: in Section II, we show the key characteristics of the DM-QCL and the MCT detector and describe the experimental setup of the FSO system.
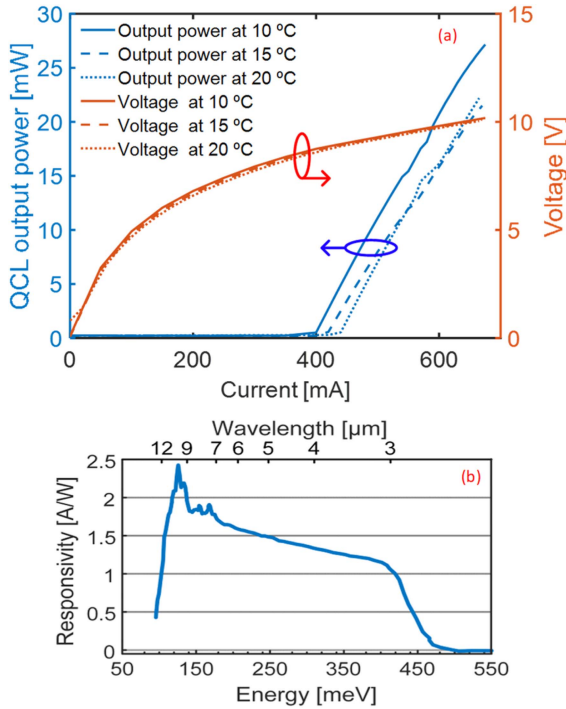
Fig. 1. (a) The measured P-I-V curves of the QCL chip at operating temperatures of 10 °C, 15 °C, and 20 °C, respectively. (b) The responsivity spectrum of the MCT detector.

Section III shows the measurement results of the LWIR transmissions with different modulation formats. Finally, a conclusion is given in Section IV.

II. EXPERIMENTAL CONFIGURATION

A. Characteristics of DM-QCL Chip and MCT Detector

The DM-QCL chip in this work is grown by molecular beam epitaxy on an InP cladding. The active region is based on a strain-compensated AlInAs/GaInAs structure. A high-reflectivity coating (>95%) is used on the back-facet while the front facet is left as-cleaved. The single-mode distributed-feedback laser is obtained through a top metal grating [21] with a coupling efficiency $\kappa \approx 4$ cm^{-1}. The 4 mm long laser is processed using a buried configuration: after etching the ridge waveguide, an Iron-doped InP regrowth is performed to enable continuous-wave (CW) operation at room temperature. The laser is mounted epi-up on an Aluminum-Nitride submount. Fig. 1(a) shows the P-I-V curves of the DM-QCL chip at operating temperatures of 10 °C, 15 °C, and 20 °C, respectively. It can be observed that the DM-QCL under CW operation has a lasing threshold of around 420 mA and this threshold slightly increases with the higher operating temperature. Note that the higher bias current requirement is certainly having an impact on the thermal stability of the optoelectronics device for real applications. A minor intersection is observed between the P-I curves at 15 °C and 20 °C, represented by the dotted and dashed lines respectively. This intersection is, however, negligible and does not significantly influence the overall interpretation of the data. When the laser bias current is up to 670 mA, the DM-QCL chip has an output

power of up to 27 mW at 10 °C. The responsivity spectrum of the MCT detector is shown in Fig. 1(b). It covers a wide operational spectral range over MWIR and LWIR, in contrast to QCD which often has a relatively narrower responsivity spectral range [13]. The transmitter beam radius is about 3 mm measured by an IR detector card. The DM-QCL emitted mode profile is a Gaussian-like profile.

B. Experimental Setup of the LWIR FSO System

Fig. 2(a) shows the experimental setup of the LWIR FSO transmission system. The detailed digital signal processing (DSP) routines in the transmitter and receiver are shown in Fig. 2(b) and (c). For system performance evaluation, we use OOK and PAM symbol sequences that are mapped from a random binary sequence of >1 million samples generated from the DSP routine in MATLAB using the Mersenne Twister with a shuffled seed number. To pre-compensate the system bandwidth limit, a root-raised-cosine pulse shaping filter with a roll-off factor of 0.15 and a static 2-tap pre-equalization filter are applied to the symbols. We optimize the tap weight according to the system BER performance, which is found to be around -0.8. After that, the tap weight is kept constant to ensure an effective pre-compensation of the frequency roll-off of the broadband signals in our transmission experiments [15]. A 50 GSa/s arbitrary waveform generator (AWG) is used to convert the digital samples generated offline into the analog domain. The DM-QCL chip with a center wavelength of 9.15 μm is mounted on a water-cooled commercial QCL mount with a Peltier thermoelectric cooler (TEC). We use a commercial MCT detector integrated with a TIA at the receiver side. With the help of an IR power meter at the receiver end, we calibrate the received signal power, optimize it, and replace the power meter with the MCT detector to convert the optical signals to electrical signals. We use the IR power meter to measure the link loss, which is 3 dB and mainly induced by the misalignment and the beam divergence. The beam divergence impacts the link loss and LWIR FSO transmission performance. A 40 GSa/s real-time digital storage oscilloscope (DSO) converts the received electrical signal to digital samples for offline processing. The received signal is processed with a matched filter, timing recovery, down-sampling process based on maximum variance, a symbol-spaced DFE with different feedforward (FF) taps and feedback (FB) configuration taps, and the BER performance is counted after the offline demodulation. The actual photos of the QCL mount, MCT detector, and part of the system setup are given in Fig. 2(d)–(f), respectively.

Fig. 3 shows the calibrated end-to-end channel amplitude response of the FSO system measured at 10 °C, 15 °C, and 20 °C including the AWG, the DM-QCL, the MCT detector, the DSO, and all the electrical components. The end-to-end 3-dB bandwidth is around 170 MHz, and the 10-dB bandwidth is about 520 MHz. One should note that despite the lower operating temperature of DM-QCL is achieved by the TEC module, the system bandwidth is not enhanced and limited by the MCT detector. However, together with the superior noise performance of the MCT detector and effective post-digital
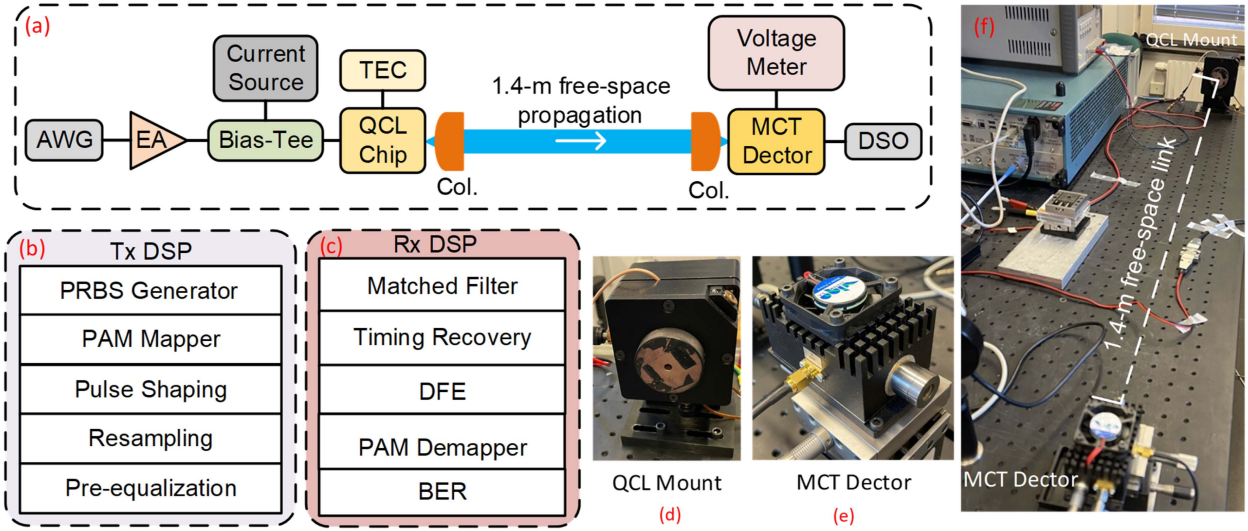
Fig. 2. The experimental setup and DSP routines in transmitter and receiver. AWG: Arbitrary waveform generator; EA: Electrical amplifier; TEC: Thermoelectric cooler; QCL: Quantum cascade laser; MCT: Mercury cadmium telluride; DSO; digital storage oscilloscope; PRBS: Pseudo random binary sequence; PAM: Pulse amplitude modulation; DFE: Decision feedback equalizer; Col.: Collimator; BER: Bit error rate.
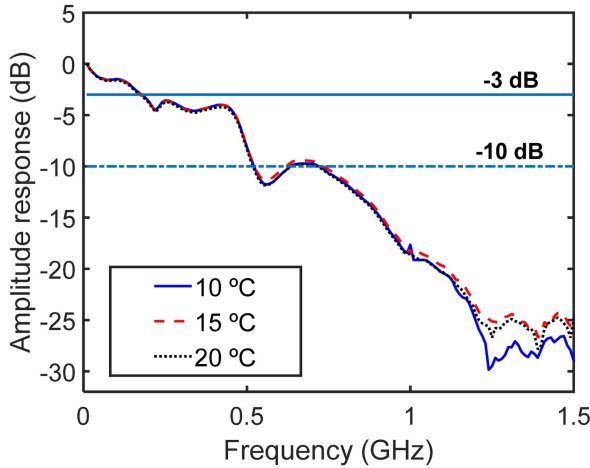

Fig. 3. Characterized end-to-end amplitude response, including the DM-QCL, MCT detector, and all the electrical components.

equalization, this FSO channel can support up to gigabaud signal transmission.

III. EXPERIMENTAL RESULTS AND DISCUSSION

In this section, we study the transmission performance with four modulation formats, including OOK, PAM4, PAM6, and PAM8. The DFE-based post-equalization is used to compensate for the signal distortions caused by the bandwidth-limited links. We optimize the BER performance with the different equalizer structures for each modulation format. The 6.25% OH HD-FEC limit is used for performance benchmarking. Besides, the KR-FEC is adopted only for the 4.5 Gbaud OOK signal.

A. On-Off Keying

Firstly, we explore the highest baud OOK transmission with achievable BER against two HD-FEC thresholds, i.e., the 6.25%
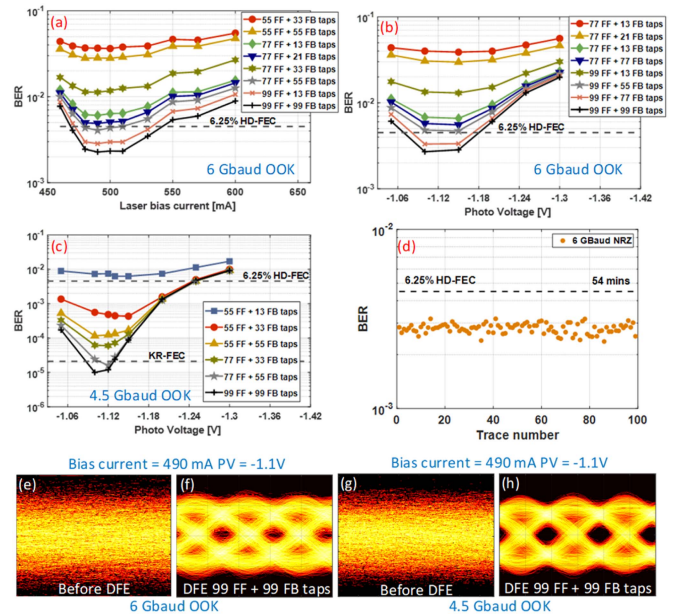

Fig. 4. (a) BER as a function of the laser bias current for 6 Gbaud OOK signal. BER as a function of the MCT detector PV for (b) 6 Gbaud and (c) 4.5 Gbaud OOK signals. (d) System stability test result. Selected eye diagrams of (e) (f) 6 Gbaud and (g)(h) 4.5 Gbaud OOK signals before or after DFE.

OH HD-FEC limit of 4.5×10^{-3} and the KR-FEC limit of 2×10^{-5}. After optimizing the beam alignment and keeping the -1.1 V of PV at the MCT detector, we evaluate the performance of the system transmission by sweeping the laser bias current of the DM-QCL. Fig. 4(a) shows the measured BER performance as a function of the laser bias current for the 6 Gbaud OOK signal. The optimal laser bias current where the lowest BER is achieved is around 490 mA. Around the optimal bias point, BER performances below the 6.25% OH HD-FEC limit are achievable with DFE consisting of 77 FF taps and 55 FB taps. After that, we sweep the PV at the detector with the optimal laser bias current
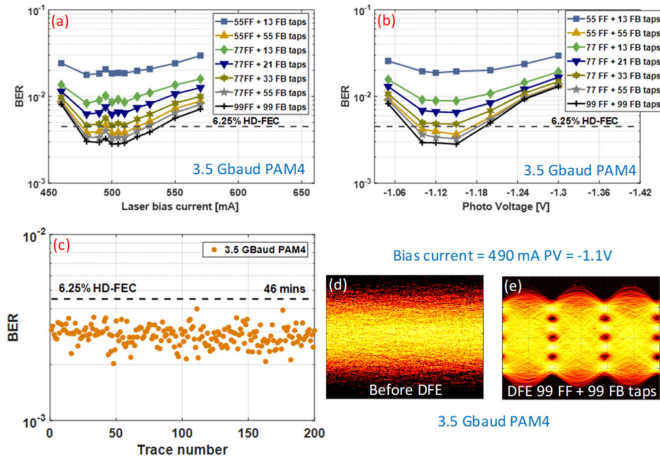
Fig. 5.   BER as a function of (a) the laser bias current and (b) the MCT detector PV for 3.5 Gbaud PAM4 signal. (c) System stability test result. (d) (e) Selected eye diagram of 3.5 Gbaud PAM4 signal before or after DFE.
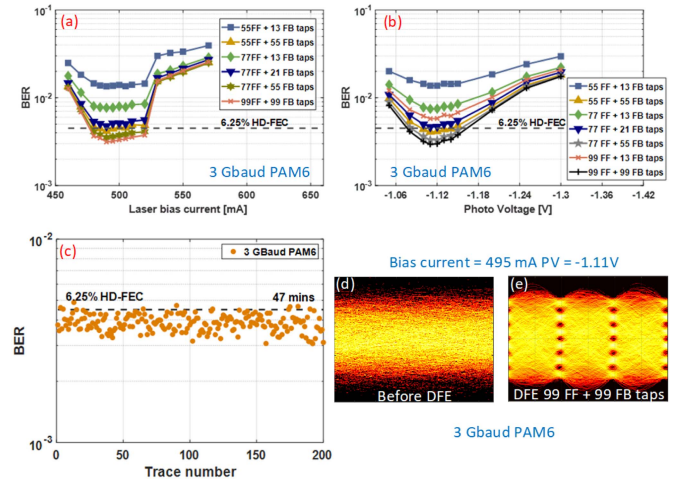

Fig. 6.   BER as a function of (a) the laser bias current and (b) the MCT detector PV for 3 Gbaud PAM6 signal. (c) System stability test result. (d) (e) Selected eye diagram of 3 Gbaud PAM6 signal before or after DFE.

to 490 mA. Fig. 4(b) and (c) show the BER as a function of the PV for 6 Gbaud and 4.5 Gbaud OOK signals, respectively. The optimal PV is around -1.12 V for both data rates. For the 6 Gbaud OOK signal, the BER performances below the 6.25%-OH HD-FEC limit are achievable with DFE consisting of 99 FF taps and 77 FB taps. We can achieve a below KR-FEC limit performance for the 4.5 Gbaud OOK signal with 77 FF and 55 FB taps.

With the increased PV at the MCT detector, the degrading BER performance occurs, mainly attributed to the system's bandwidth shrinkage mentioned in our previous work [15]. One can observe that optimizing BER is a result of a trade-off between signals' extinction ratio, the DM-QCL characteristics and received optical power. Therefore, the optimization of bias current and PV at the MCT detector is necessary for the experiment targeting to improve the BER performance. We evaluate the stability performance of the transmission for the 6 Gbaud OOK signal and show the result in Fig. 4(d). The stability test approach can be found in our previous work [17]. In this case, BERs of all traces are equalized by the DFE with 99 FF and 99 FB taps below the 6.25% OH HD-FEC limit, indicating a stable performance for the DM-QCL-based transmitter and the MCT detector. In addition, selected eye diagrams before or after DFE for both data rates at the optimal laser bias current and the MCT detector PV are shown in Fig. 4(e)–(h). After DFE, clear eye opening with negligible nonlinear distortions is observed.

B. Pulse Amplitude Modulation

We then extend our system performance evaluation with multilevel PAM signals, reflecting SNR characteristics and improving spectral efficiency. Three PAM signals, namely, PAM4, PAM6, and PAM8, are employed for this study. We explore the maximum supportable baud rate by the system setup for each modulation format, with BER performance fulfilling the 6.25% OH HD-FEC threshold requirement. Fig. 5(a) shows the BER performance as a function of the laser bias current for the 3.5 Gbaud PAM4 signal. One can be observed that the BER can

reach below the 6.25% OH HD-FEC threshold with the laser bias current around 490 mA using the DFE with more than 55 FF taps and 55 FB taps. The BER performance degrading is mainly caused by the modulation nonlinearity of the DM-QCL when the laser bias current is higher than 540 mA. With the optimal laser bias current of 490 mA, the BER performance is measured by sweeping the PV at the detector. Fig. 5(b) shows the BER performance as a function of the PV at the MCT detector using different DFE configurations. One can see that the optimal PV is also about -1.12V, and we can achieve BERs below the 6.25% OH HD-FEC limit with more than 55 FF and 55 FB taps. The stability performance of the transmission for the 3.5 Gbaud PAM4 signal is also tested. Fig. 5(c) shows the stability test result with the DFE consisting of 99 FF taps and 99 FB taps. All traces are detected with BER performance below the 6.25% OH HD-FEC limit. Fig. 5(d) and (e) show the eye diagrams before or after the DFE at the optimal laser bias and PV point to further verify the transmission performance.

Next, Fig. 6(a) shows the BER performance as a function of the laser bias current for the 3 Gbaud PAM6 signal. The optimal laser bias current was found between 480 mA and 510 mA. The 3 Gbaud PAM6 signal transmission could achieve BER values that meet the 6.25% OH HD-FEC requirement using the DFE with more than 55 FF taps and 55 FB taps. Further decreasing the equalization taps, DFE with 77 FF and 21 FB taps fails to achieve BER performance below the targeted FEC threshold of 4.5×10^{-3} BER. It can be observed that the DFE approach with larger FB taps can mitigate the inter-symbol interference of the PAM6 signal caused by the limited bandwidth of the LWIR FSO transmission system. Besides, with the increased laser bias current, the BER performance degrades quickly, indicating that higher modulation linearity and channel SNR are required for the PAM6 signals. Then, we move on to the BER test with optimal laser bias point to further optimize the PV at the detector. Fig. 6(b) shows the BER performance as a function of the PV at the MCT detector using different DFE structures. As can be seen, the optimal PV is about -1.12V. The BERs below 6.25%
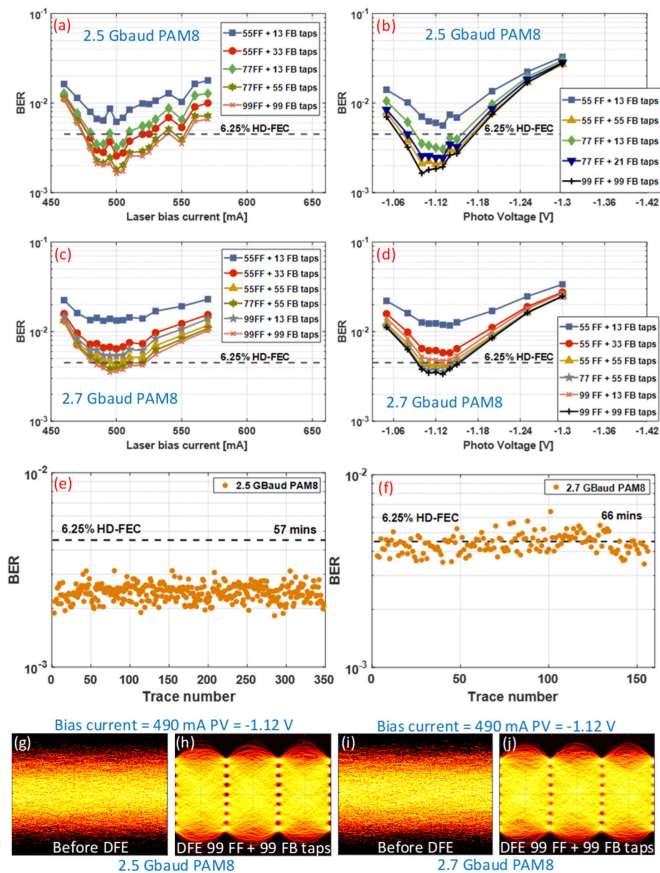
Fig. 7. BER as a function of (a) the laser bias current and (b) MCT detector PV for 2.5 Gbaud PAM8 signals. BER as a function of (c) the laser bias current and (d) the MCT detector PV for 2.7 Gbaud PAM8 signal. (e) (f) System stability test results. Selected eye diagrams of (g) (h) 2.5 Gbaud and (i) (j) 2.7 Gbaud PAM8 signals before or after DFE.

OH HD-FEC limit are achieved by using DFE with more than 55 FF and 55 FB taps. Figs. 6(c)–(e) show the system's stability and selected eye diagrams before or after DFE measured at the optimal bias current and PV point.

Finally, we adopt the PAM8 signal in the LWIR FSO transmission system to optimize spectral efficiency and bit rate further. Fig. 7(a) and (c) show the BER performance as a function of the laser bias current for the 2.5 Gbaud and 2.7 Gbaud PAM8 signals, respectively. The optimal laser bias current is located at about 500 mA. These two PAM8 signals could achieve BER below the 6.25% OH HD-FEC limit using the DFE with 77 FF and 13 FB taps and 55 FF and 55 FB taps, respectively. With the decreasing the DFE taps, BER performance below the targeted FEC threshold of 4.5×10^{-3} BER cannot be achieved. One can see that the DFE with a larger number of FB taps ($>$ 55) is required to mitigate the impairment of the 2.7 Gbaud PAM8 signal because of the limited bandwidth of the LWIR FSO transmission system. Such 8-level signals with high SNR are successfully demodulated thanks to the advanced characteristic of the QCL-based transmitter and the MCT detector. After the optimization of the laser bias point, the BER test is performed to further optimize the PV at the MCT detector. Fig. 7(b) and (d) show the BER performance as a function of the PV at the

MCT detector using different DFE structures. The results show that the optimal PV is about -1.12V, consistent with the other PAM signals. The system's stability and selected eye diagrams are also measured at the optimal bias and MCT detector PV point. Fig. 7(e)–(j) show the measured stability and selected eye diagrams before or after DFE at the optimal bias current and MCT detector PV point. It should be noted that some outliers with marginally higher BER than the 6.25% OH HD-FEC limits are detected, which is attributed to the slight power fluctuation caused by the vibrations during the measurement period. For practical application, the trade-off between the system performance and post-equalization complexity should be considered. When approaching that state, a systematic optimization process focusing on hardware design and packaging to reduce equalization complexity is expected. In addition, a wide temperature range should be supported without uncooled devices when considering practical deployment in FSO systems, which requires further research combining material engineering, device design optimization, and enhanced thermal management techniques.

IV. CONCLUSION

This study highlights the potential of LWIR FSO transmission using a DM-QCL and a commercial MCT detector. By optimizing the laser bias current and MCT detector PV, we were able to achieve a bit error rate performance below the 6.25% OH HD-FEC limit for four modulation formats, including 6 Gbaud OOK, 3.5 Gbaud PAM4, 3 Gbaud PAM6, and 2.5 or 2.7 Gbaud PAM8 signals. Additionally, the 4.5 Gbaud OOK signal was tested with results below the KR-FEC threshold. The selected eye diagrams for all modulation formats demonstrated the transmission performance of the system, and its stability was tested in a quasi-real-time manner. Considering the 6.25% FEC overhead and stability results, the LWIR FSO system achieved net data rate results up to 5.62 Gbit/s OOK, 6.56 Gbit/s PAM4, 7.03 Gbit/s PAM6, and 7.03 Gbit/s PAM8 signal transmissions. Our results indicate that the DM-QCL and MCT detector-based FSO transceivers hold immense promise for future FSO communications, providing high spectral efficiency and a potential role in future terrestrial and space communication systems.

REFERENCES

[1] X. Pang et al., "Bridging the terahertz gap: Photonics-assisted free-space communications from the submillimeter-wave to the mid-infrared," *J. Lightw. Technol.*, vol. 40, no. 10, pp. 3149–3162, May 2022.

[2] H. D. Le and A. T. Pham, "Link-layer retransmission-based error-control protocols in FSO communications: A survey," *IEEE Commun. Surv. Tut.*, vol. 24, no. 3, pp. 1602–1633, Thirdquarter 2022.

[3] S. Li, L. Yang, J. Zhang, P. S. Bithas, T. A. Tsiftsis, and M.-S. Alouini, "Mixed THz/FSO relaying systems: Statistical analysis and performance evaluation," *IEEE Trans. Wireless Commun.*, vol. 21, no. 12, pp. 10996–11010, Dec. 2022.

[4] R. Zhang et al., "Turbulence-resilient pilot-assisted self-coherent free-space optical communications using automatic optoelectronic mixing of many modes," *Nature Photon.*, vol. 15, no. 10, pp. 743–750, 2021.

[5] A. S. Hamza, J. S. Deogun, and D. R. Alexander, "Classification framework for free space optical communication links and systems," *IEEE Commun. Surveys Tut.*, vol. 21, no. 2, pp. 1346–1382, Secondquarter 2019.

[6] A. Delga and L. Leviandier, "Free-space optical communications with quantum cascade lasers," *Proc. SPIE*, vol. 10926, pp. 140–155, 2019.

[7] K. Zou et al., "High-capacity free-space optical communications using wavelength- and mode-division-multiplexing in the mid-infrared region," *Nature Commun.*, vol. 13, no. 1, Dec. 2022, Art. no. 7662.

[8] S. Yulong et al., "10 Gbps DPSK transmission over free-space link in the mid-infrared," *Opt. Exp.*, vol. 26, no. 26, pp. 34515–34528, 2018.

[9] F. Grillot et al., "Bridging the 100 GHz-10 THz domain with unipolar quantum optoelectronics," *Proc. SPIE*, vol. 12230, pp. 42–48, 2022.

[10] J. J. Liu, B. L. Stann, K. K. Klett, P. S. Cho, and P. M. Pellegrino, "Mid and long-wave infrared free-space optical communication," *Proc. SPIE*, vol. 11133, 2019, Art. no. 1113302.

[11] H. Dely et al., "10 Gbit s^{-1} free space data transmission at 9 μm wavelength with unipolar quantum optoelectronics," *Laser Photon. Rev.*, vol. 16, no. 2, 2021, Art. no. 2100414.

[12] P. Didier et al., "High-capacity free-space optical link in the midinfrared thermal atmospheric windows using unipolar quantum devices," *Proc. SPIE*, vol. 4, no. 5, 2022, Art. no. 056004.

[13] M. Joharifar et al., "High-speed 9.6-μm long-wave infrared free-space transmission with a directly-modulated QCL and a fully-passive QCD," *J. Lightw. Technol.*, vol. 41, no. 4, pp. 1087–1094, Feb. 2023.

[14] X. Pang et al., "Free-space communications enabled by quantum cascade lasers," *Physica Status Solidi (a)*, vol. 218, no. 3, 2021, Art. no. 2000407.

[15] X. Pang et al., "Direct modulation and free-space transmissions of up to 6 Gbps multilevel signals with a 4.65-μm quantum cascade laser at room temperature," *J. Lightw. Technol.*, vol. 40, no. 8, pp. 2370–2377, Apr. 2022.

[16] O. Spitz et al., "Free-space communication with directly modulated mid-infrared quantum cascade devices," *IEEE J. Sel. Topics Quantum Electron.*, vol. 28, no. 1, Jan./Feb. 2022, Art. no. 1200109.

[17] X. Pang et al., "Gigabit free-space multi-level signal transmission with a mid-infrared quantum cascade laser operating at room temperature," *Opt. Lett.*, vol. 42, no. 18, pp. 3646–3649, Sep. 2017.

[18] R. Puerta et al., "NR conformance testing of analog radio-over-LWIR FSO fronthaul link for 6G distributed MIMO networks," in *Proc. Opt. Fiber Commun. Conf.*, 2023, Paper Th2A.32.

[19] M. Joharifar et al., "8.1 Gbps PAM8 long-wave IR FSO transmission using a 9.15-μm directly-modulated QCL with an MCT detector," in *Proc. Opt. Fiber Commun. Conf.*, 2023, Paper Th1H.1.

[20] L. M. Zhang and F. R. Kschischang, "Staircase codes with 6% to 33% overhead," *J. Lightw. Technol.*, vol. 32, no. 10, pp. 1999–2002, May 2014.

[21] M. Carras et al., "Room-temperature continuous-wave metal grating distributed feedback quantum cascade lasers," *Appl. Phys. Lett.*, vol. 96, no. 16, 2010, Art. no. 161105.